Solar-Terrestrial Physics. 2021. Vol. 7. Iss. 4. P. 98–103. DOI: 10.12737/stp-74202111. © 2021 M.V. Globa, S.V. Lesovoi. Published by INFRA-M Academic Publishing House. Original Russian version: M.V. Globa, S.V. Lesovoi, published in Solnechno-zemnaya fizika. 2021. Vol. 7. Iss. 4. P. 104–110. DOI: 10.12737/szf-74202111. © 2021 INFRA-M Academic Publishing House (Nauchno-Izdatelskii Tsentr INFRA-M)

Received July 02, 2021
Accepted September 28, 2021

CALIBRATION OF SIBERIAN RADIOHELIOGRAPH ANTENNA GAINS USING REDUNDANCY

M.V. Globa
Institute of Solar-Terrestrial Physics SB RAS, Irkutsk, Russia, globa@iszf.irk.ru

S.V. Lesovoi
Institute of Solar-Terrestrial Physics SB RAS, Irkutsk, Russia, svlesovoi@gmail.com

Abstract. The paper describes application of standard gain calibration using redundancy for a 48-antenna prototype of Siberian Radioheliograph. Traditionally, for calibration, the visibilities were measured only between adjacent antennas since they have the highest signal-to-noise ratio and are sufficient for phase calibration. We have shown that this limited set of visibilities did not allow using the antenna array redundancy potential and obtaining images with a high dynamic range on a permanent basis. Images without amplitude calibration contain many artifacts and require special care when analyzed. The inclusion of visibility measurement between antennas with a double step made it possible to significantly increase the accuracy of solving the system of equations for amplitudes. Images constructed using both phase and amplitude calibrations do not have visible artifacts and are more reliable.

Keywords: solar radio telescope, visibility function, radio interferometer, gain calibration.

INTRODUCTION

Current problems of solar radio astronomy, such as the study of weak activity, place ever higher demands on the quality of images. Expanding the dynamic range and increasing the fidelity of radio interferometer images require us to improve calibration and data deconvolution (such as CLEAN etc.) methods. Calibration of complex gains, which distort visibilities measured by an interferometer, is a high-priority task in radio imaging. The choice of a particular method depends on the instrument and the object under observation. For stellar radio interferometers with high sensitivity and small angles of view the most acceptable calibration method is to observe well-known stable point sources. The rough calibration result is then, as a rule, refined using self-calibration [Cornwell, Fomalont, 1989].

When designing the Siberian Radio Heliograph (SRH) [Altyntsev et al., 2020] and its 48-antenna prototype (SRH-48) [Lesovoi et al., 2012; Lesovoi et al., 2017], it was taken into account that it is impossible to observe point sources because of insufficient sensitivity, and self-calibration is difficult when observing the quiet Sun as it requires selecting a model of brightness distribution over the solar disk. For these reasons and in view of the existing infrastructure of the Siberian Solar Radio Telescope (SSRT) [Grechnev, 2003], redundant T-shaped array configurations were chosen. Redundancy means the presence of several antenna pairs measuring the same component of the spatial spectrum of brightness distribution. Calibration with redundancy does not require additional observations of well-known stable sources, and also does not require fitting the model of brightness distribution over the solar disk. The first works on calibration with redundancy were carried out for the Westerbork Synthesis Radio Telescope (WSRT) [Noordam, de Bruyn, 1982; Wieringa, 1992], and then this method was successfully applied to the Nobeyama Radioheliograph [Nakajima et al., 1994].

SRH-48 was in operation from 2016 to 2021. The data obtained until 2020 was mainly used with phase correction only. Phase errors most strongly affect an image. This is due to the fact that at the same phase and amplitude measurement accuracy (say, 10 %) the distortions caused by phase errors reduce the dynamic range of an image much more dramatically. On the other hand, amplitude errors are usually smaller than phase errors, so only phase correction is sufficient for adequate imaging. To get images with a large dynamic range, it is also necessary to make amplitude correction.

We describe a method of calibration with redundancy in general terms and its application to SRH-48. The amplitude correction is shown to be impossible without measuring visibilities with a double step. We illustrate the result using simulated and actual SRH-48 data.

METHOD OF CALIBRATION WITH REDUNDANCY

In general, the visibilities measured by each pair of interferometer antennas can be written as follows:

$$\tilde{V}_{kl}(t) = g_k(t) g_l^*(t) G_{kl}(t) V_{kl}(t) + \varepsilon_{kl}(t) + \epsilon_{kl}(t), \qquad (1)$$

where $\tilde{V}_{kl}$ is the visibility measured by antennas k and l; V_{kl} is the true visibility; g_k is the complex gain of the kth antenna; G_{kl} is the measured visibility error unresolved into factors associated with antennas; ε_{kl} is the additive constant component for the antenna pair k and l; ϵ_{kl} is thermal noise with zero mean [Thompson et al., 2003; Cornwell, Fomalont, 1989]. Ignoring the errors related to a particular

antenna pair k, l, we write the equation for visibility in a simplified form:

$$\tilde{V}_{kl}(t) = g_k(t) g_l^*(t) V_{kl}(t) + \epsilon_{kl}(t). \quad (2)$$

Calibration is reduced to solving system of equations (2) for g. The number of equations usually exceeds manifold the number of unknowns, and all possible redundant visibilities are involved in the solution to reduce the effect of noise. To simplify further analysis, we will consider the signal-to-noise ratio high enough to neglect the terms ϵ_{kl}.

The simplest method for solving system of equations (2) is to take the logarithm of all values, which allows us to write independent linear equations for phases and amplitudes [Wieringa, 1992; Liu et al., 2010]. Antenna gains and visibilities can be represented as

$$g_k(t) = e^{a_k(t) + i\phi_k(t)}, \quad (3)$$

$$V_{kl}(t) = e^{S_{kl}(t) + i\psi_{kl}(t)}. \quad (4)$$

Then expression (2), after taking the logarithm, is as follows:

$$\tilde{S}_{kl}(t) + i\tilde{\psi}_{kl}(t) = a_k(t) + a_l(t) + S_{kl}(t) + \\ + i(\phi_k(t) - \phi_l(t) + \psi_{kl}(t)). \quad (5)$$

This form makes it possible to separate equations for phases and amplitudes and perform calibration independently:

$$\tilde{\psi}_{kl}(t) = \phi_k(t) - \phi_l(t) + \psi_{kl}(t), \quad (6)$$

$$\tilde{S}_{kl}(t) = a_k(t) + a_l(t) + S_{kl}(t). \quad (7)$$

PECULIARITIES OF APPLICATION OF CALIBRATION WITH REDUNDANCY TO SRH-48

The use of antenna array redundancy implies that a system of equations will include "redundant" visibilities, i.e. visibilities measured by manifold different but equally spaced antenna pairs. SRH-48 is a T-shaped equidistant antenna array with the shortest baseline of 4.9 m, consisting of East–West (32 antennas) and South (16 antennas) arms. For imaging, "cross" visibilities, i.e. visibilities measured by antennas of different arms, are used. Redundant visibilities are measured only for calibration. The arms do not have common antennas, since they intersect in half baseline; therefore, systems of equations for these arms are independent. Routine phase calibration involves solving two systems of equations for redundant visibilities and then correcting cross visibilities, using antenna phases found. The maximum possible number of equations for one arm is $N(N-1)/2$, where N is the number of antennas in the arm. The calibration source for SRH-48 is the Sun itself since the sensitivity of SRH-48 is insufficient to observe cosmic point sources. For the solution to be stable, the visibilities included in the system of equations should be measured with an acceptable signal-to-noise ratio $s/n > 5$ [Wieringa, 1992; Hjellming, Basart, 1982]. The solar disk has a decaying spatial spectrum; therefore, the signal level in different antenna pairs depends on the baseline distance. The strongest signal is generally recorded at the shortest baselines; and with an increase in the baseline, the signal level decreases sharply; therefore, for phase calibration of SRH-48, only the visibilities measured by pairs of adjacent antennas are used. The number of measured visibilities is also limited to hardware resources of the SRH-48 correlator. The number of equations when using only the shortest baselines is $N-1$. We show below that such a limited set of equations gives an acceptable imaging solution for phases, but for amplitudes an additional set of equations is needed.

By way of illustration, consider an array of four antennas located along one line with equal spacing. Using this array as an example, we describe the calibration method employed for SRH-48. Set up a system of equations of the form of (6) for the shortest baselines, i.e. for $l=k+1$. Only one unique visibility phase, denoted by ψ, will be included in the system of equations. Write the system of equations for phases in the matrix form

$$\begin{pmatrix} 1 & -1 & 0 & 0 & 1 \\ 0 & 1 & -1 & 0 & 1 \\ 0 & 0 & 1 & -1 & 1 \end{pmatrix} \begin{pmatrix} \phi_1 \\ \phi_2 \\ \phi_3 \\ \phi_4 \\ \psi \end{pmatrix} = \begin{pmatrix} \tilde{\psi}_{12} \\ \tilde{\psi}_{23} \\ \tilde{\psi}_{34} \end{pmatrix}. \quad (8)$$

Denoting the matrix of coefficients by $\mathbf{P}_1$, the vector of unknown phases by $\mathbf{x}$, and the resulting vector by $\mathbf{d}$, expression (8) can be written shorter: $\mathbf{P}_1\mathbf{x}=\mathbf{d}$. Obviously, system (8) has an infinite set of solutions as it contains five unknowns and three equations. In other words, there is a vector or a family of null-space vectors $\mathbf{P}_1$. This means that when multiplying such a vector with the matrix $\mathbf{P}_1$ the resulting vector will be zero. Hence, when added to the found solution of system of equations (8), this vector will have no effect. The family of null-space vectors $\mathbf{P}_1$ takes the form

$$\begin{pmatrix} \phi_1 \\ \phi_2 \\ \phi_3 \\ \phi_4 \\ \psi \end{pmatrix} = C_1 \begin{pmatrix} 1 \\ 1 \\ 1 \\ 1 \\ 0 \end{pmatrix} + C_2 \begin{pmatrix} 1 \\ 2 \\ 3 \\ 4 \\ 1 \end{pmatrix}, \quad (9)$$

where C_1 and C_2 are arbitrary constants. Addition of the first part of vector (9) to the solution ($C_1 \neq 0$; $C_2 = 0$) corresponds to addition of a constant to all phases of antenna gains, which does not play a role in correcting the visibilities measured along one arm since there are only phase differences in (8). But, as mentioned above, SRH-48 consists of two arms that do not have common antennas, and in solutions for different arms the constants C_1 will generally be different. This will lead to constant addition to phases of cross-visibilities, which will be manifested in "skew" of brightness across the solar disk and the sky in the image plane. This degeneracy can be eliminated by analyzing the image and its histogram, or by adding an equation for the shortest cross-visibility and binding the two sets of equations together into one. However, the latter method requires an assumption

about the cross-visibility phase, which can also be a source of error. The second part of vector (9) (C_1=0; $C_2\neq0$) corresponds to introducing a linear slope into phases of antenna gains, which, during subsequent correction of cross visibilities, will lead to a shift of the entire image relative to the phase center. This does not affect the dynamic range of the image and is eliminated during further processing by the procedure for centering of the solar disk.

Apply this method to amplitude calibration. The system of equations for our example of an array of four antennas will be similar to system (8), except for the signs:

$$\begin{pmatrix} 1 & 1 & 0 & 0 & 1 \\ 0 & 1 & 1 & 0 & 1 \\ 0 & 0 & 1 & 1 & 1 \end{pmatrix} \begin{pmatrix} a_1 \\ a_2 \\ a_3 \\ a_4 \\ S \end{pmatrix} = \begin{pmatrix} \tilde{S}_{12} \\ \tilde{S}_{23} \\ \tilde{S}_{34} \end{pmatrix}. \quad (10)$$

Denote the matrix by $\mathbf{A}_1$. The family of null-space vectors $\mathbf{A}_1$, as in the case of $\mathbf{P}_1$ for phases, consists of two parts:

$$\begin{pmatrix} a_1 \\ a_2 \\ a_3 \\ a_4 \\ S \end{pmatrix} = C_1 \begin{pmatrix} 1 \\ 1 \\ 1 \\ 1 \\ -2 \end{pmatrix} + C_2 \begin{pmatrix} -1 \\ 1 \\ -1 \\ 1 \\ 0 \end{pmatrix}. \quad (11)$$

Remember that in this case we deal with logarithms of amplitudes, so the addition actually means multiplication. Adding the first part of vector (11) to the solution is equivalent to multiplying moduli of gains of all antennas by an arbitrary constant and simultaneously dividing the amplitude of true visibility by the square of this constant. Consequently, during the correction all cross-visibilities are multiplied by the same arbitrary factors actually consisting of two factors for different arms, which entails a change in the integral over the image corresponding to the total solar flux at this frequency. The image is related to the total flux during further processing by referencing the brightness temperature of the solar disk to a known value. For this reason, multiplying visibilities by a constant does not affect the image quality. Adding the second part of vector (11) to the solution means multiplying moduli of gains of all antennas with even indices and dividing the moduli of gains of all antennas with odd indices by a constant, which give rise to a comb on the spectral plane (*uv* plane). The comb in the spectrum amplifies the farthest side lobes and produces false images that may overlap with the real image.

A solution containing such degeneracy severely limits the dynamic range of an image. When analyzing the left-hand side of vector (11), we can see that the comb-like degeneracy arises due to the fact that in (10) we always deal with the sum of logarithms of moduli of gains of two adjacent antennas. Hence we can assume that adding equations for double-spaced antenna pairs (1–3 and 2–4) would remove this degeneracy. Add two new equations to system (10). A new unknown visibility amplitude also appears, designated S_1 for the shortest baselines and S_2 for double baselines.

$$\begin{pmatrix} 1 & 1 & 0 & 0 & 1 & 0 \\ 0 & 1 & 1 & 0 & 1 & 0 \\ 0 & 0 & 1 & 1 & 1 & 0 \\ 1 & 0 & 1 & 0 & 0 & 1 \\ 0 & 1 & 0 & 1 & 0 & 1 \end{pmatrix} \begin{pmatrix} a_1 \\ a_2 \\ a_3 \\ a_4 \\ S_1 \\ S_2 \end{pmatrix} = \begin{pmatrix} \tilde{S}_{12} \\ \tilde{S}_{23} \\ \tilde{S}_{34} \\ \tilde{S}_{13} \\ \tilde{S}_{24} \end{pmatrix}. \quad (12)$$

The form of the null-space vector clearly implies that now only the constant remains as the only possible degeneracy.

$$\begin{pmatrix} a_1 \\ a_2 \\ a_3 \\ a_4 \\ S_1 \\ S_2 \end{pmatrix} = C \begin{pmatrix} 1 \\ 1 \\ 1 \\ 1 \\ -2 \\ -2 \end{pmatrix}. \quad (13)$$

As mentioned above, the presence of a constant in visibilities is of no import, so now the solution for amplitudes may be considered accurate.

Note that the additional equations radically change the accuracy of the amplitude calibration, and for phases the equations with double baselines have no effect on vector (9). This is due to the fact that the additional equations for phases are not linearly independent. Moreover, in order to solve a system with equations for different baseline distances, the logarithmic approach requires phase unwrapping such that the behavior of the right-hand side of equation (6) is linear. At a wide spread of antenna gain phases, as well as at different values of solar visibility phases, this might be difficult. In such cases, it is preferable to use nonlinear methods and to solve the system of equations of type (2) in a complex form, although they need more computational resources.

For the above reasons, the choice of equations only for the shortest baselines, in view of their highest signal-to-noise ratio for phase calibration of SRH-48 data, seems optimal. Amplitude calibration requires the additional use of equations for double baselines. Note, however, that the signal level in double baselines may change significantly over time. Figure 1 illustrates the behavior of the visibility function modulus for the shortest double baselines, measured at different frequencies from the beginning of the observations to the noon. These baselines measure the low-frequency part of the spatial spectrum, where the response to the solar disk dominates. In the domain of spatial frequencies, the response to the circular disk is the Airy disk — the Bessel function of the first kind divided by its argument. During the day, the position of the baseline vector on the spectral plane changes and at some moments gets close to the first and second zeros of the Bessel function. This causes the signal-to-noise ratio to drop below 5, and visibilities become unsuitable for calibration. For such cases, it is preferable to use the calibration obtained at the nearest moment in time, when all visibilities in the system of equations have a sufficient signal-to-noise ratio.

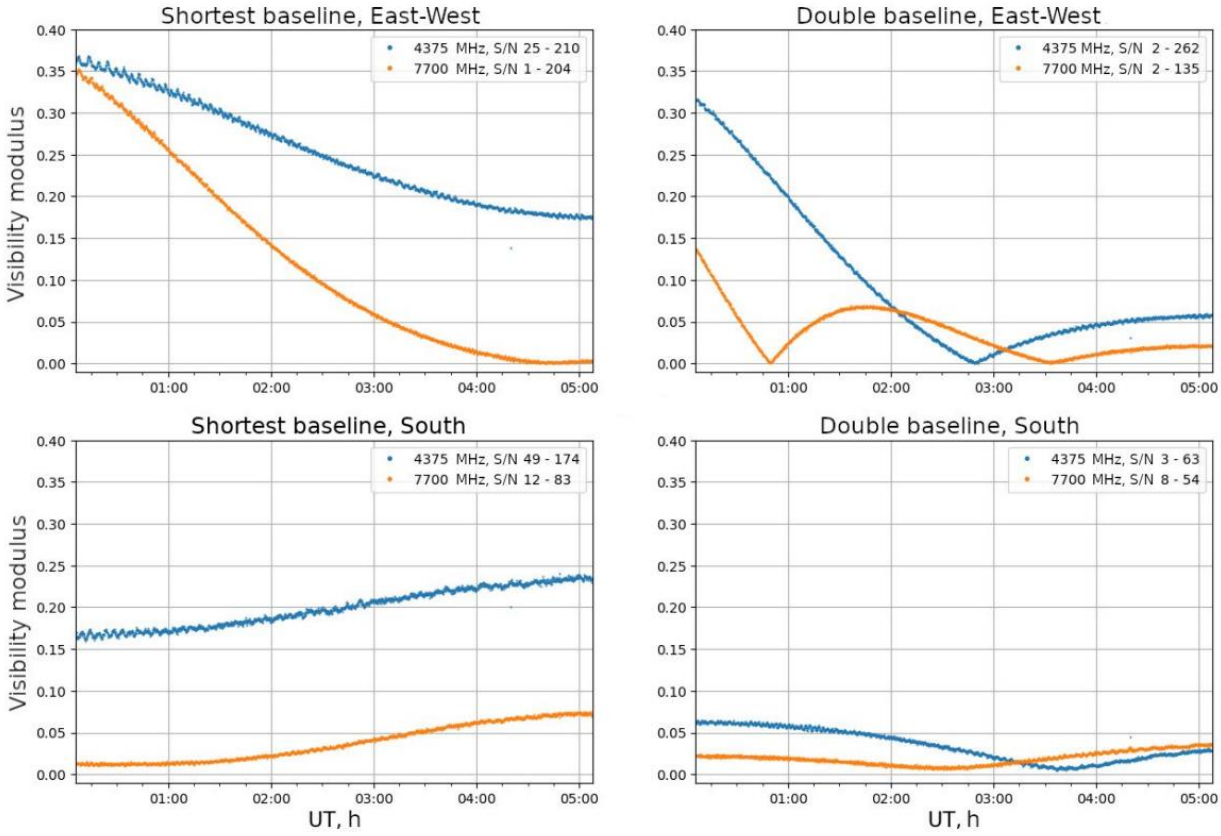

Figure 1. Signal level variation in different baselines of the East–West and South arms from the beginning of observations to noon for May 10, 2020. Blue color marks 4375 MHz; orange, 7700 MHz. For each curve, minimum and maximum values of the signal-to-noise ratio are given.

AMPLITUDE CALIBRATION OF SRH-48 DATA

The result described in the previous section can be shown by simulated data representing the computed components of the spatial spectrum of the solar model, which correspond to cross and redundant antenna pairs for a particular point in time. Each spectral component is multiplied by specified complex gains measuring this component. The above calibration method is applied to the resulting set of visibilities to calculate antenna gains and restore the original spectral components. Figure 2 presents the result of calculation of gains for 32 antennas of the East–West arm. The comb appears explicitly when the original moduli of antenna gains are divided by the gain moduli calculated using only the shortest baselines. When we add equations for double baselines, only a constant remains.

Redundant visibilities for double-spaced antenna pairs have been recorded by SRH-48 from March 9, 2020. Previously recorded data was generally used without amplitude calibration. Figure 3 illustrates the effect of amplitude calibration of the data on a solar image and its histogram, used for referencing to brightness temperatures. Images are shown in the coordinate system of direction cosines (l, m). The solar images forming at adjacent maxima of the SRH-48 beam have the opposite sign due to the array configuration. Images with phase and amplitude correction for short baselines exhibit artifacts that distort images and their histograms. This reduces the accuracy of referencing brightness temperatures of the disk and determining brightness temperatures of sources. At higher frequencies, disk temperature distortions may be even greater since artifacts overlap with the true image. The last image, obtained using amplitude calibration for short and double baselines, does not contain such artifacts. This means that the image is close to convolution with an ideal beam and the CLEAN algorithm works more accurately. Figure 4 shows dirty and clean images of the quiet Sun, taken on May 3, 2020 at 6125 MHz. Cleaning an extended object such as the Sun is a separate challenge and is beyond the scope of this work. In this case, a simple algorithm of subtracting the response to the disk and cleaning the remaining bright areas with the Högbom algorithm was adopted [Högbom, 1974]. By comparison, we present an image for the same day obtained by SDO/AIA at a wavelength of 304 Å. The dynamic range of SRH-48 images is 50:1 and 156:1 respectively. Without amplitude calibration and cleaning, the dynamic range is 5:1. Figure 5 gives an example of cleaning a bright source during an M1.2 class flare without amplitude calibration (left) and with amplitude calibration (right). The image obtained using only phase correction contains many residual side lobes. Amplitude calibration suppresses side lobes and increases the dynamic range six times. Of particular note is that without amplitude calibration the antenna temperature of a

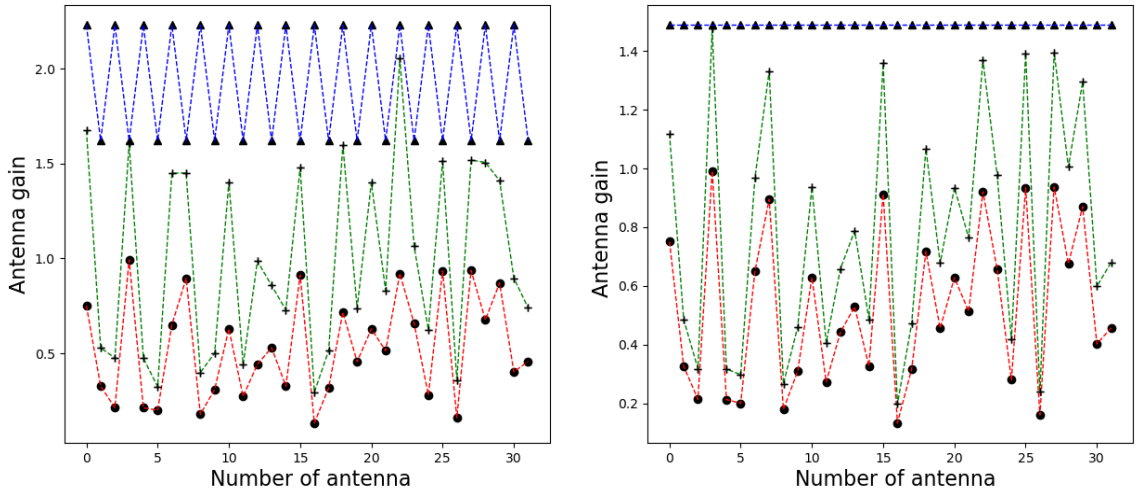

Figure 2. Result of amplitude calibration simulation. Left: dots connected by the red dotted line are original moduli of antenna gains; pluses connected by the green dotted line are calculated antenna amplitudes for only short baselines; triangles connected by the blue dotted line are their quotient indicating that the solution differs from the initial values by a constant and a comb. Right: the same for the solution with addition of double baselines

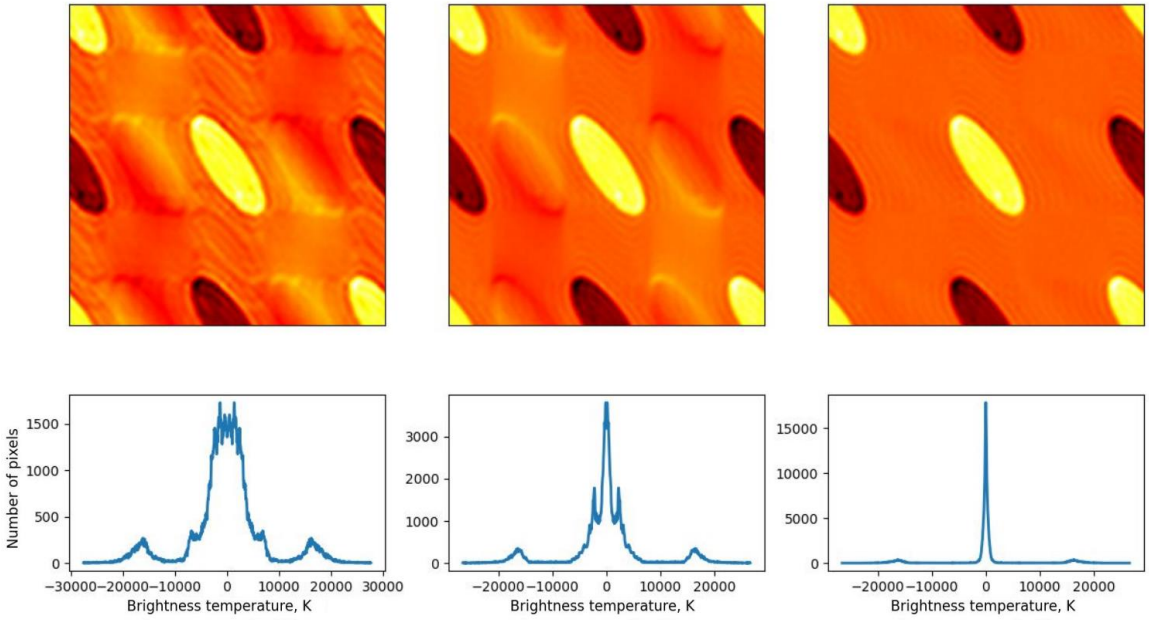

Figure 3. Effect of amplitude calibration on an image. An image after phase calibration (left); an image after phase and amplitude calibrations using only the shortest baselines (center); an image after phase and amplitude calibrations using the shortest and double baselines (right); under each image are their histograms. The images were captured on March 14, 2020 at 4300 MHz

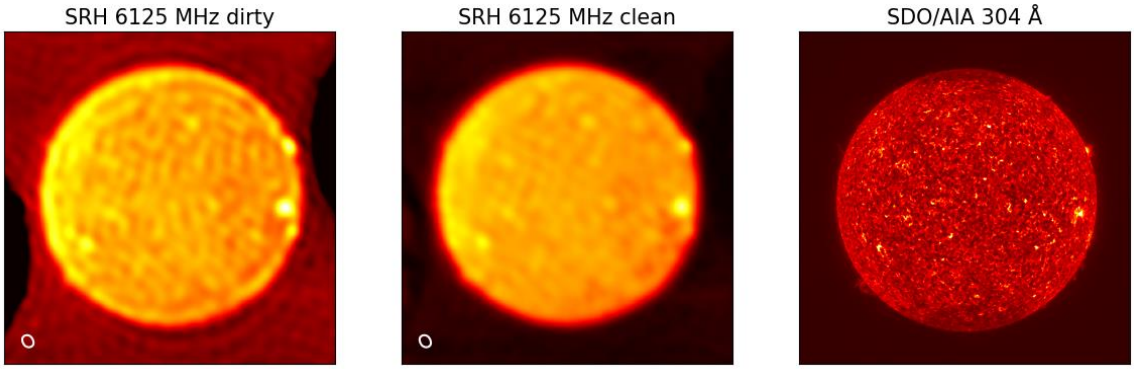

Figure 4. Solar images for May 3, 2020. A dirty image obtained at a frequency of 6125 MHz after phase and amplitude calibrations (left); the same image after cleaning bright sources and the disk (center); an SDO/AIA image at a wavelength of 304 Å (right). Size of the SRH-48 beam is shown in the lower left corner. Accumulation time is 15 s

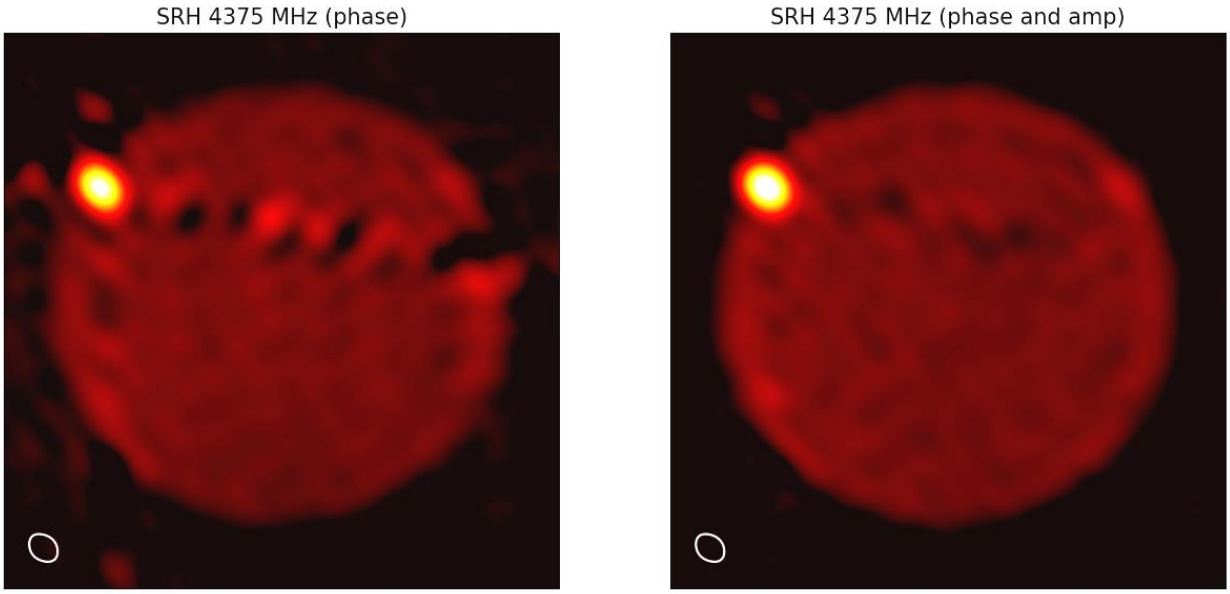

Figure 5. Clean images of an M1.2-class flare on May 29, 2020 at 07:22 UT at 4375 MHz. A phase-corrected image (left); a phase- and amplitude-corrected image (right). Accumulation time is 0.14 s. The maximum antenna temperature of the flare source is $492 \cdot 10^3$ K and $605 \cdot 10^3$ K respectively. The dynamic range is 47:1 and 290:1 respectively

source is underestimated by 18 %. There is more noise in the images than in Figure 4 because we use the shortest possible accumulation time. Residual side lobes in a phase and amplitude calibrated image can be caused by high frequency harmonic distortions in visibilities (see Figure 1) of hardware origin.

CONCLUSION

In this paper, we have implemented a method of amplitude calibration of SRH-48 antenna gains. We have shown analytically and using model data that capturing an acceptable image requires calibration with visibilities measured in the shortest and double baselines. We have reported the result of amplitude calibration of real SRH-48 data.

The work was carried out partly under Government Assignment for 2021 No. 075-00374-21-00 dated December 24, 2020 "Methods and instruments of an astrophysical experiment" (unique number 0278-2021-0010, registration number TsITiS 121040600115-2); partly using funds of the Russian Science Foundation (project No. 18-12-00172).

REFERENCES

Altyntsev A., Lesovoi S., Globa M., Gubin A., Kochanov A., Grechnev V., et al., Multiwave Siberian Radioheliograph. *Solar-Terrestrial Physics*. 2020, vol. 6, iss. 2, pp. 30–40. DOI: 10.12737/stp-62202003.

Cornwell T., Fomalont E.B. Self-calibration. *Synthesis imaging in radio astronomy*. *A Collection of Lectures from the Third NRAO Synthesis Imaging Summer School*. Published by the Astronomical Society of the Pacific. 1989, vol. 6, p. 185. San Francisco, 1989.

Grechnev V.V., Lesovoi S.V., Smolkov G.Ya., et al. The Siberian Solar Radio Telescope: the current state of the instrument, observations, and data. *Solar Phys*. 2003, vol. 216, iss. 1, pp. 239–272. DOI: 10.1023/A:1026153410061.

Hjellming R.M., Basart J.P. The theory of the instrument. *Introduction to the NRA0 Very Large Array*. Ch. 2. NRAO, 1982.

Högbom J.A. Aperture synthesis with a non-regular distribution of interferometer baselines. *Astron. Astrophys. Suppl.* 1974, vol. 15, p. 417.

Lesovoi S.V., Altyntsev A.T., Ivanov E.F. Gubin A.V. The multifrequency Siberian Radioheliograph. *Solar Phys*. 2012, vol. 280, iss. 2, pp. 651–661. DOI: 10.1007/s11207-012-0008-7.

Lesovoi S., Altyntsev A., Kochanov A., Grechnev V., Gubin A., Zhdanov D., et al. Siberian Radioheliograph: first results. *Solar Terrestrial Physics*. 2017, vol. 3, iss. 1, pp. 3–18. DOI: 10.12737/24347.

Liu A., Tegmark M., Morrison S., Lutomirski A., Zaldarriaga M. *Precision Calibration of Radio Interferometers Using Redundant Baselines.* 2010. arXiv:1001.5268. DOI: 10.1111/j. 1365-2966.2010.17174.x.

Nakajima H., Nishio M., Enome S., et al. The Nobeyama Radioheliograph. *Proc. IEEE*. 1994, vol. 82, iss. 5, pp. 705–713.

Noordam J., de Bruyn A. High dynamic range mapping of strong radio sources, with application to 3C84. *Nature*. 1982, vol. 299, iss. 5884, pp. 597–600. DOI: 10.1038/299597a0.

Perley R.A. High Dynamic Range Imaging. *Synthesis Imaging in Radio Astronomy II, A Collection of Lectures from the Sixth NRAO/NMIMT Synthesis Imaging Summer School.* ASP Conference Ser., 1999, vol. 180, pp. 275.

Thompson A.R., Moran J.M, Swenson G.W., Jr.. *Interferometry and Synthesis in Radio Astronomy*. 2nd ed. New York: Wiley, 2001. 692 p. DOI: 10.1002/9783527617845.

Wieringa M.H. An investigation of the telescope based on calibration methods ‘redundancy’ and ‘self-cal’. *Experimental Astronomy*. 1992, vol. 2, pp. 203–225. DOI: 10.1007/BF00420576.

How to cite this article

Globa M.V., Lesovoi S.V. Calibration of Siberian Radioheliograph antenna gains using redundancy. *Solar-Terrestrial Physics.* 2021. Vol. 7. Iss. 4. P. 98–103. DOI: 10.12737/stp-74202111.